Altering Conserved Lipid Binding Sites in Cytochrome *c* Oxidase of *Rhodobacter sphaeroides* Perturbs the Interaction between Subunits I and III and Promotes Suicide Inactivation of the Enzyme†

Lakshman Varanasi,‡ Denise Mills,§ Anna Murphree,‡ Jimmy Gray,‡ Chris Purser,|| Rodney Baker,|| and Jonathan Hosler*,‡

Department of Biochemistry and Department of Pharmacology and Toxicology, University of Mississippi Medical Center, 2500 North State Street, Jackson, Mississippi 39216, and Department of Biochemistry and Molecular Biology, Michigan State University, East Lansing, Michigan 48824

Received July 10, 2006; Revised Manuscript Received October 12, 2006

ABSTRACT: Subunit III of the three-subunit catalytic core of cytochrome *c* oxidase (C*c*O) contains no metal centers, but it does bind two lipids, within a deep cleft, in binding sites conserved from bacteria to humans. Subunit III binds to subunit I, where it prevents the spontaneous suicide inactivation of C*c*O by decreasing the probability of side reactions at the heme−Cu O_2 reduction site in subunit I. Subunit III prevents suicide inactivation by (1) maintaining adequate rates of proton delivery to the heme−Cu active site and (2) stabilizing the structure of the active site during turnover [Mills and Hosler (2005) *Biochemistry 44*, 4656]. Here, we first show that mutating several individual residues of the conserved lipid binding sites in subunit III disturbs the subunit I−III interface. Then, two lipid binding site mutants were constructed with an affinity tag on subunit III such that the mutant C*c*Os could be isolated with 100% subunit III. R226A eliminates an ion pair to the phosphate of the outermost lipid of the cleft, while W59A-F86A disrupts interactions with the fatty acid tails of both lipids. Once these mutant C*c*Os are placed into soybean phospholipid vesicles, where extensive exchange of bacterial for soybean lipids takes place, it is shown that altering the lipid binding sites mimics a major loss of subunit III, even though subunit III is completely retained, in that suicide inactivation becomes much more probable. The rate of proton delivery to the active site remains rapid, ruling out slow proton uptake as the primary reason for increased suicide inactivation upon alteration of the lipid binding sites. We conclude that altering the lipid binding sites of subunit III may promote side reactions leading to suicide inactivation by allowing greater movement to occur in and around the O_2 reduction site of subunit I during the catalytic cycle.

An increasing number of crystal structures of integral membrane proteins reveals that many bind lipid at specific sites using a variety of noncovalent interactions. Isolated integral membrane proteins may bind considerable amounts of lipid, but the lipids that appear in crystal structures must be bound in specific orientations with high occupancy. In cases where the crystal structure shows a multiplicity of interactions between a lipid and a protein, i.e., the presence of a lipid binding site, the status of a bound lipid advances from that of a loosely bound, annular lipid to that of a structural component of the protein (*1*−*3*). Mutagenesis of a lipid binding site in the yeast cytochrome bc_1 complex (*4*) and the photolabeling of cardiolipin binding sites in bovine cytochrome *c* oxidase (*5*) have provided experimental evidence that structural lipids may mediate protein−protein interactions within the membrane. Although it is well established that bound lipids are often required for full enzyme activity (*2*, *3*, *5*, *6*), there are few experimental determinations of the mechanisms by which structural lipids affect membrane protein function.

Cytochrome *c* oxidase (C*c*O)[1] offers a unique opportunity to study the structural and functional role of the structural lipid because the catalytic core of the multimeric enzyme contains highly conserved lipid binding sites. C*c*O spans the inner membrane of mitochondria and the cytoplasmic membrane of many aerobic bacteria, where it transfers electrons from cytochrome *c* to O_2 and uses much of the energy of electron transfer to generate a transmembrane electrical potential (*7*−*11*). The three largest subunits, I, II, and III, form the catalytic core of the enzyme. Electrons from cytochrome *c* are delivered to the dicopper Cu_A center in

† Supported by National Institutes of Health Grants GM56824 (to J.H.) and GM26916 (to S. Ferguson-Miller, Michigan State University).

* Corresponding author. Tel: 601-984-1861. Fax: 601-984-1501. E-mail: jhosler@biochem.umsmed.edu.

‡ Department of Biochemistry, University of Mississippi Medical Center.

§ Department of Biochemistry and Molecular Biology, Michigan State University.

|| Department of Pharmacology and Toxicology, University of Mississippi Medical Center.

[1] Abbreviations: C*c*O, cytochrome *c* oxidase; PE, phosphatidylethanolamine; WT, wild-type C*c*O; WT III (−), wild-type C*c*O lacking subunit III; COV, cytochrome oxidase vesicle; I-His, C*c*O form with a six-histidine tag on the C-terminus of subunit I; III-His, C*c*O form with a six-histidine tag on the N-terminus of subunit III; FCCP, carbonyl cyanide *p*-(trifluoromethoxy)phenylhydrazone; ICP-OES, inductively coupled plasma optical emission spectroscopy; SVD, singular value decomposition.

10.1021/bi061390q CCC: $33.50
Published on Web 11/23/2006

subunit II, near the outer surface of C*c*O, from which they flow to six-coordinate heme *a* in subunit I and then on to the buried heme a_3-Cu_B site in subunit I, where O_2 is reduced to water. The four protons required for the reduction of one diatomic oxygen, plus four that are simultaneously pumped through the protein, are taken up from the inner surface of C*c*O and moved ~30 Å through specific proton transfer pathways to the buried heme a_3-Cu_B active site or to the site of proton pumping, located at or near the active site (*11*, *12*). Subunit III of the three-subunit catalytic core of C*c*O is as highly conserved as subunit I (45% vs 47% identity between *Rhodobacter sphaeroides* and human subunits III and I, respectively). Despite being highly conserved, the functional role of subunit III remained enigmatic for many years, in part because the subunit is the only member of the catalytic core that contains no metal centers. More recently, it has been shown that a primary role of subunit III is to prevent, or decrease the probability of, side reactions during O_2 reduction that cause irreversible inactivation of C*c*O. This phenomenon of suicide inactivation takes place at the heme a_3-Cu_B active site (*13*) and most likely involves the self-hydroxylation of C*c*O by the oxoferryl intermediate formed during O_2 reduction (*14*).

Subunit III decreases the probability of suicide inactivation in two ways. First, it facilitates proton transfer to the active site through two pathways in subunit I, the D pathway leading from the inner surface and the proton backflow pathway leading from the outer surface (*15*). More rapid proton delivery to the active site shortens the lifetime of the oxoferryl intermediate of O_2 reduction, thereby decreasing the probability that this reactive intermediate will initiate a destructive side reaction (*14*). Second, subunit III appears to deter suicide inactivation by stabilizing the heme a_3-Cu_B active site in subunit I during catalytic turnover (*14*). This is evident from the fact that C*c*O forms inactivate far more slowly in the presence of subunit III even in cases where the delivery of protons to the active site is slow (*14*, *15*). Since subunit III is bound to a large transmembrane surface of subunit I, it is not surprising that it exerts structural influence on the active site in subunit I, also located in the transmembrane region.

Although subunit III does not contain redox centers, it does bind two structural lipids in binding sites that are extensively conserved from bacteria to mammals. The structures of *R. sphaeroides* [PDB ID 1M56 (*16*)] and bovine [PDB ID 1V54 (*17*)] C*c*O show that the seven transmembrane helices of subunit III are organized into two domains that create a deep cleft containing the two lipid binding sites (Figures 1 and 2). In the bovine C*c*O structure the lipids in these sites are phosphatidylglycerol, while in the *R. sphaeroides* structure the lipids are identified as phosphatidylethanolamines. PE1 is located at the back of the cleft (Figure 1) where it is bound by a network of noncovalent bonds from residues of both subunits I and III (Figure 2). PE2 is located in front of PE1, and it makes no direct contact with subunit I. However, residues of subunit III extend their side chains into the cleft to simultaneously contact the fatty acids of PE1 and PE2.

The C*c*O structures predict that protein−lipid interactions will form a significant part of the subunit I−III binding interaction. The experiments presented below are consistent with this prediction, but they also show that weaker protein−lipid interactions have a stronger influence on subunit I−III

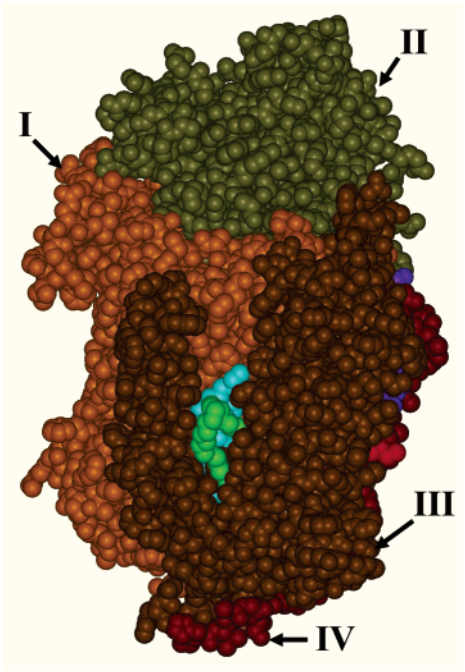

FIGURE 1: Space-filling representation of *R. sphaeroides* C*c*O showing the two phospholipids buried in the cleft of subunit III. The coordinates are from 1M56 (*16*). PE1, at the rear of the cleft, is colored as cyan, while PE2, in front of PE1, is colored green. Subunits I, III, and IV are largely within the membrane, while the portion of subunit II shown here extends into the periplasm (analogous to the intermembrane space of mitochondria) in order to bind cytochrome *c*. The two transmembrane helices of subunit II lie against subunit I opposite the face that binds subunit III. Subunit IV is a single transmembrane helix, with no direct cognate in mitochondrial C*c*O, that is associated with bound lipids on the face of C*c*O to the right.

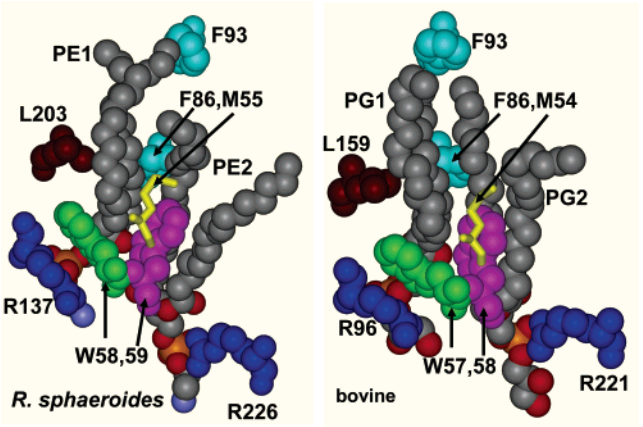

FIGURE 2: Similarity of the lipid binding sites in the cleft of subunit III of *R. sphaeroides* and bovine C*c*O. The coordinates are from 1M56 [*R. sphaeroides* (*16*)] and 1V54 [bovine (*17*)]. Shown are the two phospholipids (elemental colors) as PE in *R. sphaeroides*, PG in bovine, and some of the conserved residues that form the binding pocket for the lipids. The methionine residue is shown in stick form to enable visualization of other residues.

binding than was expected. With regard to the function of subunit III, the significant question is, what role, if any, do the structural lipids in the cleft play in preventing suicide inactivation? The results show that mutations that alter the binding sites for these lipids can promote suicide inactivation in the presence of subunit III. However, the mutations that promote suicide inactivation do not slow proton delivery to the active site to the extent required to cause the measured

increase in inactivation. This leads to the conclusion that normal lipid binding sites in subunit III are important for the subunit's ability to stabilize the active site of C*c*O during catalytic turnover and thereby prevent suicide inactivation.

MATERIALS AND METHODS

Materials. Soybean phosphatidylcholine [L-α-phosphatidylcholine (L-α-lecithin)] was purchased from Sigma and recrystallized using the procedure of Sone et al. (*18*). Sodium cholate (Anatrace) was prepared as a 10% solution in water, while *n*-dodecyl β-D-maltoside (Anatrace) was prepared as a 30% solution in water. Valinomycin and FCCP were from Sigma. Horse heart cytochrome *c* was purchased from Sigma and further purified on carboxymethylcellulose (*19*) when used as the substrate for COVs. Ni-agarose was from Qiagen.

CcO Forms Containing a Six-Histidine Tag on the C-Terminus of Subunit I. Mutations in subunit I of *R. sphaeroides* C*c*O (R137A, L145A-L196A-L203A) were constructed and expressed as described previously (*14*), using the pRK415-based (*20*) expression plasmid pAH1H32 that expresses all of the oxidase genes except for subunit IV. Mutations in subunit III were constructed and expressed as in Bratton et al. (*21*).

CcO Forms Containing a Six-Histidine Tag on the N-Terminus of Subunit III. This involved the creation of a two-plasmid expression system in *R. sphaeroides*. The first is pLH449, a pRK415-based plasmid that expresses the genes for untagged subunit I and subunit II plus the assembly proteins Cox10p (*22*) and Cox11p (*23*). To create pLH449, *coxIII* was removed from pYJ100 (*24*) as a *Sma*I fragment, and then a *Pst*I fragment from the religated vector, containing *coxII*, *cox10*, and *cox11*, was cloned into pBR322 to create pCF102b. The *Pst*I fragment was restricted from pCF102b and cloned into the *Pst*I site of pRK415 to create pLH380. A *Hin*dIII fragment containing untagged *coxI* was restricted from pCH37 (*25*) and ligated into the *Hin*dIII site of pLH380 to create pLH449, which was conjugated into *R. sphaeroides* by standard methods (*26*). The second plasmid of the system is pJG213, a pBBR1MCS-based plasmid (*27*) which expresses subunit III with a six-histidine tag at its N-terminus. A plasmid containing the *coxI* promoter, the N-terminal region of *coxI* and *lacZ*, pRKKctaD (*28*), was mutated and manipulated to remove *lacZ* and place an *Nde*I site at the ATG start codon of *coxI*, creating a pBSII KS-based plasmid named pMEG983. Independently, pMB301, containing promoterless *coxIII* in pUC19 (*21*), was mutated to introduce an *Nde*I site at the ATG start codon of *coxIII*, creating pJG110. *CoxIII* was excised from pJG110 as an *Nde*I−*Sac*I fragment and used to replace the *Nde*I−*Sac*I fragment of pMEG983. This created pJG111, which now had the *coxI* promoter in position to drive the expression of *coxIII*. A *Hin*dIII−*Sac*I fragment, containing the *coxI* promoter−*coxIII* region of pJG111, was cloned into pBBR1MCS-2, a broad-host range vector (*27*) capable of coexisting in *R. sphaeroides* along with pRK415-based vectors, to create pJG211. QuikChange was used to introduce codons into pJG211 encoding HHHHHHSA immediately following the N-terminal methionine of subunit III, creating the His-tagged subunit III expression plasmid pJG213.

To generate subunit III mutants in this system, *coxIII* was mutated directly in pJG213, and the mutant plasmids were conjugated into *R. sphaeroides* YZ200 containing pLH449. [YZ200 is a deletion strain lacking the *coxII-III* operon (*24*).] All mutations were verified by DNA sequencing. To generate double mutants with D132A, a subunit I mutation, a version of pCH37 containing the D132A mutation in *coxI*, was obtained from Dr. Carrie Hiser of Michigan State University. *CoxI*-D132A was restricted from this plasmid using *Hin*dIII and cloned into pLH380 to create pLH449/D132A. This plasmid was conjugated into *R. sphaeroides* JS100 [a deletion strain lacking the genomic copy of *coxI* (*29*)] containing either pJG213/W59A-F86A or pJG213/R226A to express W59A-F86A-D132A and R226A-D132A, respectively.

CcO Isolation and Activity Measurements. Bacterial growth and oxidase purification by Ni-affinity chromatography were performed as in Zhen et al. (*24*). The removal of subunit III, the preparation of cytochrome oxidase vesicles (COVs), proton pumping measurements, and the rate of cytochrome *c* oxidation by COVs were performed as in Mills et al. (*15*). C*c*O was resolubilized from COVs by the addition of dodecyl maltoside to 0.1% final volume. In order to repurify C*c*O from COVs for lipid extraction and analysis (below), the COVs were dissolved in 3% dodecyl maltoside and chromatographed on Ni-NTA agarose (Qiagen) as in Zhen et al. (*24*). Measurement of the rates of O_2 reduction were performed using an oxygen electrode as described previously (*14*). The measurements of catalytic life span as the CC_{50}, including data evaluation, were performed as in Mills and Hosler (*14*).

Protein Gels and Densitometry. C*c*O purified by Ni-affinity chromatography was diluted to 4 μM in a sample buffer of 4% SDS, 20% glycerol, 62.5 mM Tris-HCl, pH 6.8, and 0.05% bromophenol blue, separated on 14% polyacrylamide−0.1% SDS gels containing 6 M urea as described in ref *27*, and stained with Coomassie Blue. To analyze C*c*O from COVs, 150 μL of COVs was made 0.1% in dodecyl maltoside; the protein was precipitated with 300 μL of ice-cold 10% trichloroacetic acid and centrifuged at 16000*g* for 30 min. The pellet was washed three times with 0.3 M Tris-HCl, pH 7.4, and then resuspended in a minimal volume of the sample buffer listed above. Images of the protein gels were obtained by scanning them on a Hewlett-Packard Scanjet scanner using HP Precision Scan Pro, and densitometry of the images was performed using UN-SCAN-IT gel, version 6.1 (Silk Scientific), on a PC. The content of subunit III in the C*c*O complex was estimated from the ratio of subunit III pixels to subunit II pixels because normal C*c*O purified by a histidine tag on subunit I will contain subunits III and II in a 1:1 stoichiometry. Subunit I was not used as the internal control because the subunit I band of C*c*O purified by Ni-affinity chromatography of dissolved cytoplasmic membranes using the histidine tag on subunit I includes significant amounts of subunit I*a*, which is free subunit I containing only heme *a* (*30*). Wild-type C*c*O was run and measured on every gel.

Lipid Extraction and Formation of Fatty Acid Methyl Esters. Samples of purified C*c*O, bulk soybean lipid [L-α-phosphatidylcholine (L-α-lecithin); Sigma)], and purified cytoplasmic membranes from *R. sphaeroides* were extracted using a procedure based on the method of Bligh and Dyer (*31*). Each sample was transferred to a water/methanol/methylene chloride solution (1/2/1) and allowed to stand for 10−30 min. The mixture was converted to a two-phase

system by adding water and methylene chloride to obtain a 1/1/1 ratio. The lower, methylene chloride layer was removed to a clean glass tube and evaporated under nitrogen to near dryness. Methyl esters of the fatty acids of the extracted lipids were formed using acid-catalyzed transesterification. Dry methanol (1.0 mL) containing 10% hydrochloride gas was added to the sample, which was held at 75 °C for 20 min. The sample was then cooled on ice, and 2 mL of hexane was added followed by the gentle addition of 1 mL of 2.5 N sodium hydroxide. The hexane layer was removed to a clean tube and evaporated to dryness under nitrogen. The sample was dissolved in 200 μL of hexane for analysis by gas chromatography/mass spectrometry (GC/MS).

Analysis of Fatty Acid Methyl Esters by GC/MS. The fatty acid methyl esters were separated using a Rtx-5ms 15 m × 0.25 mm, 0.25 μm capillary column (Restek). Helium was used as the carrier gas at a constant flow of 1.5 mL/min. The injection port temperature was 200 °C, and 1.0 μL samples were introduced using the split mode at a ratio of 50/1. The oven temperature program was started at 100 °C, held at this temperature for 1 min, and then ramped at 15 °C/min to 280 °C, where it was held for 10 min. Fatty acid methyl esters were identified and their relative concentrations measured using a Voyager mass spectrometer (ThermoFinnigan) in the positive electron impact ionization mode, performing a full scan from 50 to 450 amu in 0.39 s. The emission current was 150 μA, and electron energy was at 70 eV. The source temperature was 200 °C, and the GC/MS interface temperature was 290 °C. Identification of individual fatty acid methyl esters was confirmed using the NIST Mass Spectral Search Program to access the NIST/EPA/NIH Mass Spectral Library using XCalibur software (ThermoFinnigan). The relative amounts of each fatty acid methyl ester were determined by integration of the peaks of the total ion current chromatogram using the XCalibur software package.

*Estimation of the Phospholipid Content of Purified C*c*O Forms.* Inductively coupled plasma optical emission spectroscopy (ICP-OES) using a Spectro Genesis spectrometer was used to determine the phosphorus and copper content of 2 μM samples of purified C*c*O. Three determinations were made on each sample. The phospholipid content per monomer of C*c*O was estimated by assuming one P per phospholipid and three Cu per C*c*O monomer.

RESULTS

Alteration of Conserved Lipid Binding Site Residues Leads to Substoichiometric Binding of Subunit III to Subunit I. The crystal structures of *R. sphaeroides* and bovine heart C*c*O show that the two phospholipids in the cleft of subunit III are bound and positioned by conserved residues of subunit III that extend from helix 2 of the two-helix region on one side of the cleft, from helices 3 and 6 of the five-helix bundle on the other side, and from helices 3, 4, and 5 of subunit I, which form the rear wall of the cleft (Figures 1 and 2). Alteration of these residues in *R. sphaeroides* C*c*O by site-directed mutagenesis generally resulted in decreased binding of subunit III to subunit I (Table 1). For these experiments, the mutant oxidases were isolated via a six-histidine tag on the C-terminus of subunit I, and the content of subunit III in the purified complex was determined by densitometry of Coomassie-stained protein gels (Figure 3).

Table 1: Subunit III Content of C*c*O Forms Purified by a Six-Histidine Tag on Subunit I

C*c*O I-His form	subunit	type of lipid interaction	approximate subunit III content (% relative to wild-type C*c*O)
R137A	I	ion pair	5−25
R226A	III	ion pair	∼90
W59A	III	H-bond, VdW[a] contact	50−70
W58A	III	H-bond, VdW contact	50−70
F86A	III	VdW contact	50−70
W59A-F86A	III	VdW contact	60−80
M55A	III	VdW contact	30−50
F93A	III	VdW contact	40−60
L145A-L196A-L203A	I	VdW contact	100
A205T	III	none	100
G78S	III	none	100
S89A	III	none	100

[a] Van der Waals.

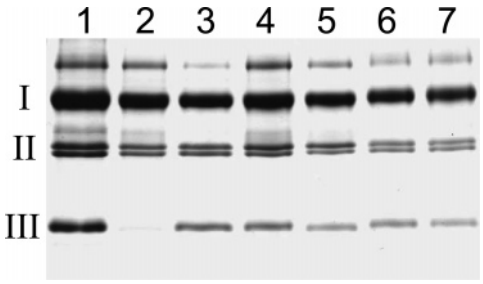

FIGURE 3: Estimating the subunit III content in C*c*O forms isolated using the histidine tag on subunit I. Densitometry was performed on numerous protein gels such as this, as described in Materials and Methods, in order to obtain the data presented in Table 1. Subunit II runs as a doublet at M_r 37 and 35 due to incomplete processing at its C-terminus (*25*); both bands of subunit II were included in the densitometry measurements. Lanes: 1, wild type; 2, R137A (showing, in this preparation, almost complete loss of subunit III); 3, W59A; 4, W58A; 5, M55A; 6, F86A; 7, F93A. See Figure 2 for the normal positions of the mutated residues in the lipid binding site of subunit III.

The crystal structures show that the phosphates of PE1 and PE2 each form an ion pair with an arginine residue. The phosphate of PE1, located toward the rear of the cleft, forms a 2.7 Å ion pair with Arg-137 of subunit I, while Arg-226 extends from helix 6 of subunit III in order for two of its guanidinium nitrogens to form an ion pair/hydrogen bond network (3.08 and 2.85 Å) with two oxygens of the phosphate of PE2 (Figure 2). The subunit III content of purified R137A was low (but variable), and the subunit III content of purified R226A was slightly less than normal (Table 1).

Two conserved tryptophan residues form hydrogen bonds with each lipid and position the proximal regions of the fatty acid tails (Figure 2). The ϵ-nitrogen of Trp-59 forms a hydrogen bond (2.9 Å) with the carbonyl oxygen of one of the fatty acids of PE1, while its indole ring intercalates between the fatty acid tails of both PE1 and PE2 to position the first 6−8 carbons of all four fatty acid tails, especially those of PE2. Trp-58 forms hydrophobic contacts with the fatty acids of PE1 only, while its ϵ-nitrogen hydrogen bonds one of the phosphate oxygens of PE1. Alteration of either Trp-59 or Trp-58 to alanine reduced the subunit III content

Table 2: V_{max} of Cytochrome *c*-Driven O_2 Reduction (pH 6.5) and Catalytic Life Spans (pH 7.4) of C*c*O Forms in Dodecyl Maltoside Solution after Purification from the Bacterial Membrane and after Solubilization from COVs

C*c*O form	V_{max} ($e^- s^{-1}$) of C*c*O forms purified from bacterial membrane[a]	V_{max} ($e^- s^{-1}$) of C*c*O forms following solubilization from COVs[a]	catalytic life span (CC_{50}) of C*c*O forms purified from bacterial membrane[b]	catalytic life span (CC_{50}) of C*c*O forms following solubilization from COVs[b]
WT I-His	1905 ± 59	not determined	$>3 \times 10^6$	$>3 \times 10^6$
WT III-His	2043 ± 43	1809 ± 63	$>3 \times 10^6$	$>3 \times 10^6$
R226A III-His	1416 ± 33	1355 ± 26	$1.65 \times 10^6 \pm 68000$	55000 ± 6500[c] (39000 ± 2000)[d]
W59A-F86A III-His	1978 ± 42	1790 ± 38	$1.57 \times 10^6 \pm 156000$	75000 ± 13000

[a] Error is standard error of the hyperbolic fit to the data. [b] Error is standard deviation of different measurements. [c] R226A III-His solubilized from COVs and repurified on Ni-agarose containing 100% subunit III. [d] R226A III-His solubilized from COVs containing 80% subunit III.

of the oxidase complex by ~30−50% (Table 1). Also in this region, conserved hydrophobic residues Met-55 and Phe-86 of subunit III extend their side chains from either side of the cleft to make simultaneous contacts with the fatty acids of both PE1 and PE2. The alteration of either Met-55 or Phe-86 to alanine also resulted in a decreased content of subunit III (Table 1).

Further up in the cleft, well-conserved residues from both subunits III and I form van der Waals contacts with the terminal regions of the fatty acids of PE1 and PE2. The side chains of Leu-145, Leu-196, and Leu-203 of subunit I contact the fatty acid tails of PE1. Simultaneous alteration of these three residues to alanine had no effect on the content of subunit III (Table 1). In contrast, the alteration of Phe-93 of subunit III, whose side chain is located near the terminal carbon of a fatty acid of PE1 (Figure 2), resulted in a significant loss of subunit III from the purified complex (Table 1).

In order to determine if the failure to assemble subunit III into the C*c*O complex is a characteristic specific of mutants affecting lipid binding residues, C*c*O forms containing alterations of subunit III residues that are not directly involved in lipid binding, and do not participate in other binding interactions with subunit I, were also analyzed. G78S and A205T are two subunit III mutants associated with mitochondrial disease (*21*). Gly-78 is located at the bottom of helix 3, in hydrophobic contact with Thr-210 of helix 4 of subunit I. Ala-205 extends its side chain into a hydrophobic region toward the top of the five-helix bundle of subunit III. Both G78S I-His and A205T I-His showed a normal subunit III content (Table 1), indicating that the introduction of more polar side chains in these positions does not affect the binding of subunit III to subunit I. Ser-89 is located in helix 3 of subunit III, within 5 Å of Leu-240 and Pro-244 of helix 5 of subunit I, but it makes no hydrogen bonds with subunit I. Its side chain hydroxyl does form a hydrogen bond (2.48 Å) with the backbone carbonyl of Phe-86. Loss of this interaction between Ser-89 and Phe-86 in S89A I-His did not affect the assembly of subunit III onto subunit I (Table 1).

*A Histidine Tag on Subunit III Allows for the Isolation of Mutant C*c*O Forms Containing Stoichiometric Amounts of Subunit III.* In order to best assess the functional consequences of altering the lipid binding sites in subunit III by site-directed mutagenesis, it was necessary to develop a system to purify C*c*O complexes containing stoichiometric amounts of mutant subunits III. This was accomplished by engineering a six-histidine tag onto the N-terminus of subunit III such that only complexes containing subunit III will bind to the Ni-affinity column. Wild-type C*c*O containing the N-terminal tag on subunit III, termed WT III-His, purified with the same yield as C*c*O containing the C-terminal tag on subunit I [(WT I-His (*24*, *32*)]. The O_2 reduction activities (Table 2) and proton pumping efficiencies (Figure 6) of WT I-His and WT III-His are essentially identical.

Subunit III affects proton uptake into the D pathway that transfer protons from the inner surface of C*c*O toward the active site (*15*, *33*, *34*). Since the histidine tag at the N-terminus of subunit III could approach surface-exposed Asp-132 of subunit I, the entry point of the D pathway, C*c*O forms containing the histidine tag on subunit III were carefully examined for possible alterations in D pathway activity. Three experiments established that the subunit III tag had no apparent effect. First, direct measurements of the rate of proton uptake into the D pathway using C*c*O forms that differed only in having the histidine tag on subunit I or subunit III showed no differences (Ädelroth and Hosler, unpublished results). Second, the pH dependence of steady-state O_2 reduction, an indicator of the pH dependence of D pathway proton uptake (*33*), was the same for both WT III-His and WT I-His [apparent pK_a ~8.4−8.5 (*15*)]. Third, this experiment takes advantage of a previous observation. The alteration of Asp-132 to alanine strongly inhibits proton uptake into the D pathway (*33*). Once subunit III is removed, however, significant rates of proton uptake and O_2 reduction are restored to D132A because the removal of a structural barrier created by the N-terminal region of subunit III allows an internal water molecule of the D pathway to function as an alternative initial proton donor/acceptor (*33*). Measurements showed that the O_2 reduction activity of D132A III (+) remained low whether the histidine tag was on subunit I or on subunit III (V_{max} of both D132A forms = 47−48 $e^- s^{-1}$ at pH 6.5). This indicates that the subunit I−III interaction around the entrance to the D pathway is no more affected by the tag on subunit III than it is by the tag on subunit I.

Two Lipid Binding Site Mutants Exhibit Rapid Suicide Inactivation after Incorporation into COVs. Two mutant C*c*Os with a subunit III histidine tag were created for extensive functional analysis. As explained above, Arg-226 ion pairs with the phosphate of PE2 (Figure 2), and its alteration to alanine, creating R226A III-His, eliminates the strongest individual bond binding PE2 to subunit III. The double mutant W59A-F86A III-His was created to eliminate a hydrogen bond to PE1 and multiple van der Waals interactions with the fatty acids of both cleft lipids (Figure 2). These mutations did not prevent the production of active enzyme. As isolated from the Ni-affinity column, the maximum rates of O_2 reduction exhibited by R226A III-His and W59A-F86A III-His were only slightly less than that of wild-type C*c*O (Table 2).

The complete removal of subunit III increases the tendency of C*c*O to suicide inactivate as a result of spontaneous structural alterations at the heme a_3-Cu_B active site during catalytic turnover (*13*). The removal of subunit III increases the probability of suicide inactivation by slowing proton uptake; slower proton delivery to the active site increases the lifetime of reactive O_2 reduction intermediates during the catalytic cycle (*14*). In addition, the analysis of inactivating C*c*O forms indicates that the presence of subunit III provides structural stability to the active site during catalytic turnover, and the loss of this stabilizing influence upon the removal of subunit III also promotes suicide inactivation (see Discussion for details). The measure of suicide inactivation is the catalytic life span, also designated the CC_{50}. The CC_{50} is the average catalytic life span of the C*c*O form, in terms of catalytic cycles (not time), where one catalytic cycle is defined as $1O_2 \rightarrow 2H_2O$. For example, a CC_{50} of 10000 (a short life span) indicates that every C*c*O monomer in the population performs an average of 10000 catalytic cycles before it irreversibly inactivates.

Wild-type C*c*O exhibits a long catalytic life span of $>3 \times 10^6$ catalytic cycles. As purified from the Ni-affinity column, the catalytic life spans of R226A III-His and W59A-F86A III-His were approximately 2-fold lower, indicating that the mutations increased the probability of suicide inactivation (Table 2). Once these two mutants were incorporated into phospholipid vesicles composed of soybean phospholipids, a striking change was noted: their catalytic life spans were greatly reduced, indicating a much higher probability of suicide inactivation. This phenotype persisted as the lipid binding site mutants were returned to their detergent-solubilized form using 0.1% dodecyl maltoside (Table 2). Detergent-solubilized soybean phospholipids were included during COV resolubilization so that the enzymes would not be depleted of lipid. In contrast to the mutants, the catalytic life span of wild-type C*c*O was unaffected by COV incorporation and resolubilization (Table 2).

In order to determine if the alteration of subunit III residues outside of the lipid binding sites would promote suicide inactivation to the same extent as R226A III-His and W59A-F86A III-His, the catalytic life spans of A205T I-His, G78S I-His, and S89A I-His (described above) were determined. The life spans of all three of these mutants were similar to that of wild-type C*c*O, even after COV incorporation and resolubilization (data not shown).

Is the Increased Suicide Inactivation Exhibited by the Lipid Binding Site Mutants Caused by the Loss of Subunit III? It was considered that the greatly increased probability of suicide inactivation exhibited by R226A III-His and W59A-F86A III-His could have resulted from the removal of subunit III during their incorporation into COVs or their subsequent resolubilization with dodecyl maltoside. Both protein gels and an activity assay specific for the presence of subunit III demonstrated the complete retention of subunit III by W59A-F86A III-His and at least 80% retention of subunit III by R226A III-His. The basis of the activity assay, a highly sensitive test for the loss of subunit III, has been introduced above. Briefly, the subunit I mutation D132A strongly inhibits C*c*O activity by inhibiting proton uptake into the D pathway (*33*, *35*). The removal of subunit III restores significant O_2 reduction activity to D132A by allowing an alternative route for proton input into the pathway (*15*, *33*).

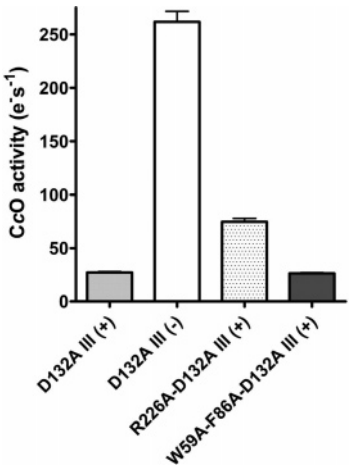

FIGURE 4: O_2 reduction activity of D132A III-His, D132A III (−), R226A-D132A III-His, and W59A-R226A-D132A III-His after solubilization from COVs. Assays were performed at pH 7.4, as described in Materials and Methods, using 40 μM horse heart cytochrome *c* as substrate. Error is standard deviation.

In order to take advantage of this behavior to test for the loss of subunit III, the double and triple mutants R226A-D132A III-His and W59A-F86A-D132A III-His were created and assayed. W59A-F86A-D132A III-His showed the same O_2 reduction activity as D132A III-His alone, after both C*c*O forms had been incorporated into COVs and then redissolved into dodecyl maltoside (Figure 4). This indicated that subunit III of W59A-F86A-D132A III-His was completely retained upon its passage through COVs. If the subunit had been released, increased O_2 reduction activity would have been observed. This result agreed with protein gels (not presented) of W59A-F86A III-His after its solubilization from COVs, which showed complete retention of subunit III. The activity exhibited by R226A-D132A III-His after COV incorporation and resolubilization was slightly greater than that of D132A III-His (Figure 4), indicating some loss of subunit III from R226A-D132A III-His. The increase in activity was ~20% of the difference in activities between D132A III-His and D132A III (−), which corresponds to a 20% loss of subunit III from R226A-D132A III-His. Again, this result agreed with protein gels (not presented). Given that R226A III-His as resolubilized from COVs is actually a mixture of 80% R226A III-His and 20% WT III (−), with an overall catalytic life span of 39000 catalytic cycles (CC; Table 2), along with the knowledge that WT III (−) shows a life span ~10000 CC under these conditions (*14*), simple calculations indicated that the R226A III-His in this mixture must have a catalytic life span ~50000 CC. This was proven by purifying the resolubilized mutant on Ni-agarose, which recaptures only C*c*O containing stoichiometric amounts of subunit III since the histidine tag is located on this subunit. The measured catalytic life span of R226A III-His repurified from COVs was 55000 CC (Table 2), in good agreement with the calculated value. Thus, both lipid binding site mutants, in the presence of 100% subunit III, exhibited catalytic life spans that were only 1.8−2.5% the life span of normal C*c*O.

Does Inhibition of Proton Uptake into the D Pathways of the Lipid Binding Site Mutants Cause the Increase in Suicide Inactivation? The fact that the lipid binding site mutants lose no more O_2 reduction activity than wild-type C*c*O after their incorporation into COVs (Table 2) argues that slow proton uptake into the D pathway cannot be the cause of the 20−

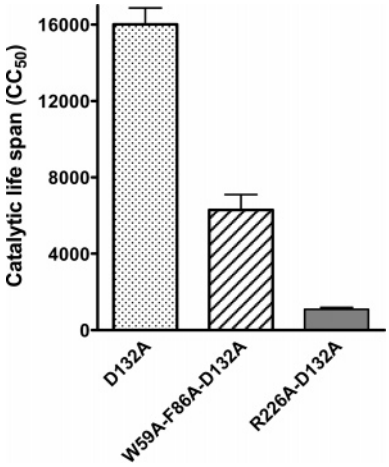

FIGURE 5: Catalytic life spans of D132A III-His, W59A-F86A-D132A III-His, and R226A-D132A III-His after solubilization from COVs. Assays were performed as described in Materials and Methods. Error is standard deviation.

30-fold increase in suicide inactivation that occurs upon the passage of these mutants through COVs. However, the absolute rate of O_2 reduction exhibited by R226A III-His is ~30% lower than that of WT III-His (Table 2); W59A-F86A III-His has the same activity as wild-type C*c*O. Since the maximum rate of C*c*O turnover (~2000 e^- s^{-1}; Table 2) is five times less than the maximum possible rate of proton uptake into the D pathway [~10000 H^+ s^{-1} (*12*)], it is possible for D pathway activity to be inhibited without a large decrease in the rate of steady-state O_2 reduction.

In order to test if the increased probability of suicide inactivation exhibited by the two lipid binding site mutants could have resulted solely from slower proton uptake into the D pathway, the catalytic life spans of the C*c*O forms that combined the D132A mutation with the lipid binding site mutations were measured. The rationale for this experiment is as follows. The mutation of Asp-132 to alanine essentially eliminates D pathway activity (*33*), but a slow rate of O_2 reduction activity persists due to a limited backflow of protons from the outer surface of C*c*O to the active site (*15*, *36*). The single mutant D132A III-His has a short catalytic life span of ~16000 catalytic cycles even in the presence of subunit III, due to very slow proton delivery to the active site (Figure 5) (*14*, *33*). Since the D132A mutation so strongly inhibits proton uptake by the D pathway, any additional slowing of proton uptake caused by the R226A and W59A-F86A mutations in subunit III should not further shorten the catalytic life span if suicide inactivation by R226A III-His and W59A-F86A III-His results from inhibition of the D pathway. If, however, the lipid binding site mutations increased the probability of suicide inactivation by some mechanism other than inhibition of the D pathway, the combination of the D pathway mutation with the lipid binding site mutations should create C*c*O forms with a shorter catalytic life span than D132A alone. The latter was found to be true: both R226A-D132A III-His and W59A-F86A-D132A III-His had significantly shorter life spans than D132A III-His, after all of the C*c*O forms were incorporated into COVs and then resolubilized (Figure 5). Thus, some process other than inhibition of the D pathway must contribute to the decreased catalytic life span caused by mutating the lipid binding sites in the cleft of subunit III.

Table 3: Stopped-Flow Measurements of Controlled and Uncontrolled Electron Transfer Rates (Cytochrome *c* Oxidation) of C*c*O Forms in COVs

COVs	controlled activity[a]	uncontrolled activity[b]	uncontrolled/ controlled
WT III-His	78 ± 4	482 ± 37	6.2
WT III (−)[c]	11 ± 1	390 ± 26	35
R226A III-His	64 ± 4	466 ± 23	7.3
W56A-F86A III-His	86 ± 4	547 ± 18	6.4

[a] Units are electrons s^{-1}. Standard errors are from the differences in rates from SVD analysis and fitting of the individual data sets of at least three measurements. Final reagent concentrations were 8 μM prereduced cyt c^{2+}, 0.2 μM aa_3 in COVs, and 2 μM valinomycin. [b] Final reagent concentrations were the same as for the controlled experiment except for the addition of FCCP to 5 μM. [c] Data from Mills et al. (*15*).

Does Inhibition of Proton Backflow in the Lipid Binding Site Mutants Cause the Increase in Suicide Inactivation? When C*c*O is incorporated into closed phospholipid vesicles (COVs) and soluble cytochrome *c* delivers electrons to the exposed outer surface of the enzyme, catalytic turnover rapidly generates a membrane potential that slows "normal" proton uptake from the inner surface. This slows the rate of O_2 reduction. This slower rate of "controlled" O_2 reduction is partially dependent upon the uptake of protons from the outer surface of C*c*O, through a proton backflow pathway that may be the proton exit pathway operating in reverse (*11*, *37*). The complete removal of subunit III inhibits proton backflow, suggesting that a region of subunit III, quite distinct from that which interacts with the D pathway at the inner surface, helps to maintain the structure of the backflow pathway in subunit I (*15*). If proton backflow from the outer surface of C*c*O is inhibited at the same time that proton uptake from the inner surface via the D pathway is inhibited, increased suicide inactivation may result, even in the presence of subunit III (*14*). Inhibition of proton backflow is characterized by a slower than normal rate of controlled electron transfer in COVs, with a corresponding rise in the ratio of the rate of uncontrolled turnover (using uncouplers or detergent to remove the membrane potential) to the rate of controlled turnover (Table 3) (*15*).

The ratio of the rates of uncontrolled vs controlled O_2 reduction was not elevated for R226A III-His or W59A-F86A III-His COVs, as it is for WT III (−) COVs (Table 3). Thus, mutation of the lipid binding sites in the cleft of subunit III had little or no effect on proton backflow from the outer surface of subunit I to the active site, and reduced proton backflow cannot be a source of increased suicide inactivation in these mutants.

Effect of the Lipid Binding Site Mutations on Proton Pumping. Along with promoting suicide inactivation, the removal of subunit III decreases the efficiency of proton pumping by C*c*O (*15*). The efficiency of proton pumping by R226A III-His was considerably lower than that of wild-type C*c*O (Figure 6). In fact, the H^+/e^- of R226A III-His was as low as WT III (−) (*33*, *34*). In contrast, W59A-F86A III-His showed a normal efficiency of proton pumping (Figure 6).

Phospholipid Exchange Occurs upon Incorporation of CcO into COVs. The types of phospholipid bound to *R. sphaeroides* C*c*O, as purified from bacterial membranes by Ni-affinity chromatography, include phosphatidylcholine, phosphatidylethanolamine, phosphatidylglycerol, and perhaps

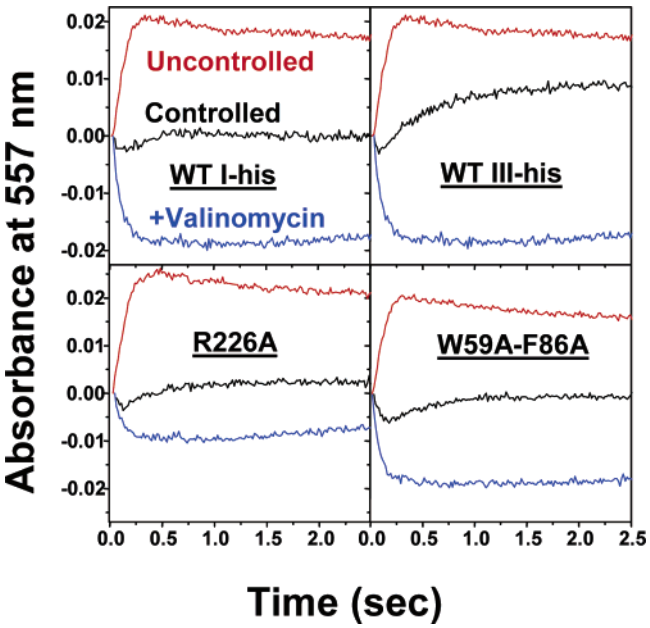

FIGURE 6: Proton pumping by COVs containing WT I-His, WT III-His, R226A III-His, and W59A-F86A III-His. Measurements were performed in 50 μM Hepes−KOH, pH 7.4, 45 mM KCl, and 100 μM phenol red using an Olis-rsm stopped-flow spectrophotometer as in ref *37*. Acidification on the outside of the COVs due to proton pumping (blue line) is seen as a decrease in the absorbance of phenol red. The addition of 2 μM valinomycin is necessary to collapse the electrical potential which otherwise opposes the extrusion of protons, as seen in the controlled state (black line) where no ionophores are present. The net alkalinization, due to the consumption of protons during O_2 reduction, is seen as an absorbance increase in the uncontrolled state (red line), produced by the presence of both 2 μM valinomycin and 5 μM FCCP, which collapses the electrical potential and allows protons to rapidly equilibrate across the membrane. Since one electron is consumed for every proton consumed during O_2 reduction, the ratio of the amplitudes of these two phenol red absorbance changes gives the stoichiometry of proton pumping as protons pumped per electron transferred. The H^+/e^- values were as follows: WT I-His, 0.92; WT III-His, 0.91; R226A III-His, 0.38; W59A-F86A III-His, 0.96.

phosphatidylserine (*38*). Sulfolipid and galactolipid are also present (*38*). In this study, the number of phospholipids bound to purified wild-type C*c*O averaged 22 ± 4 per C*c*O monomer (n = 7), as determined from measurements of phosphorus and copper by ICP-OES, using the copper content as the measure of C*c*O monomers (three Cu per C*c*O monomer). This total includes the two phospholipids bound in the cleft of subunit III. Ni-purified R226A III-His showed the same amount of bound phospholipid. The phospholipid content of both wild-type C*c*O and R226A III-His was unchanged from 22 per monomer following their repurification from COVs using Ni-affinity chromatography (see Materials and Methods).

Even though the number of phospholipids bound to C*c*O remains the same following the passage of the enzyme complex through COVs, extensive exchange of soybean for bacterial lipids takes place. The fatty acids of the lipids of the bacterial cytoplasmic membrane are predominantly oleic (18:1), while linoleic (18:2) acid was not observed (Figure 7). In contrast, the lipids of soybean lecithin, the source of the lipids used to prepare COVs, contain large amounts of 18:2 fatty acids and a lower content of 18:1 fatty acids (Figure 7). These differences allow estimation of the extent of lipid exchange. Fatty acid profiles were determined by GC/MS, following methylation of the fatty acids cleaved from extracted lipids (see Materials and Methods). This procedure allows quantitative determination of the percentages of different fatty acid species since the high chemical similarity of the fatty acids allows each to respond in a uniform manner to methylation, release from the GC column, and ionization in the mass spectrometer (*39*−*41*). As originally isolated from the Ni-affinity column, the fatty acid profiles of wild-type C*c*O and R226A III-His are the same as that of the bulk lipids present in the cytoplasmic membrane (Figure 7). The 18:1 fatty acids comprise 76% of the total, and 18:2 fatty acids are absent. After repurification of these C*c*O forms from COVs, the fatty acid profiles of their bound lipids are highly similar to that of the soybean lipid used to prepare COVs. The 18:2 fatty acids, originally absent, predominate, while the 18:1 fatty acid content drops from 76% to 24%, the same as that seen in bulk soybean lipid.

DISCUSSION

Protein−*Lipid*−*Protein Interactions Involving the Lipids in the Cleft of Subunit III Are Important for Binding Subunit III to Subunit I.* The structural importance of the protein−lipid interactions seen in the structure of the four-subunit aa_3-type C*c*O of *R. sphaeroides* has been tested by site-directed mutagenesis. In the protein−lipid−protein network between subunits I and III, the side chain of Arg-137 of subunit I forms an ion pair with a phosphate oxygen of PE1, while Trp-59, Trp-58, Met-55, and Phe-86 and other residues of subunit III make hydrogen bonds and/or hydrophobic interactions with PE1 and PE2 (Figure 2). The importance of this network in binding subunit III to subunit I is apparent from the finding that altering any one of these interactions reduces the amount of subunit III in the C*c*O complex isolated via an affinity tag on subunit I. Of particular interest is the finding that the mutation of subunit III residues involved only in weak, hydrophobic interactions with the cleft lipids, such as Met-55, Phe-86, and Phe-93, significantly affects the binding of subunit III to subunit I. This suggests that positioning of the fatty acid tails in the cleft is important for the formation of strong interactions between subunits I and III, most obviously the ion pair between Arg-137 of subunit I and the phosphate oxygen of PE1. It is also interesting that removing weak protein−lipid interactions formed by residues of subunit III (Phe-86, Phe-93) affects the binding of subunit III to subunit I (Table 1), while removing weak interactions formed by residues of subunit I (Leu-145, Leu-196, Leu-203) does not. Such a hierarchy could indicate an order of assembly for the lipids into the binding sites of the cleft.

The Arg-137-PE1 ion pair is clearly an important part of the total interaction between subunits I and III, as evidenced by the finding that the isolated R137A I-His complex contains less subunit III than any other single mutation tested thus far (Table 1). A similar protein−lipid−protein connection has been demonstrated as essential for the interaction of cytochrome c_1 and the Rieske protein of the detergent-solubilized cytochrome bc_1 complex of yeast (*4*).

Alteration of the Lipid Binding Sites in the Cleft of Subunit III Induces Suicide Inactivation, Similar to the Removal of Subunit III. Previous studies have demonstrated that a

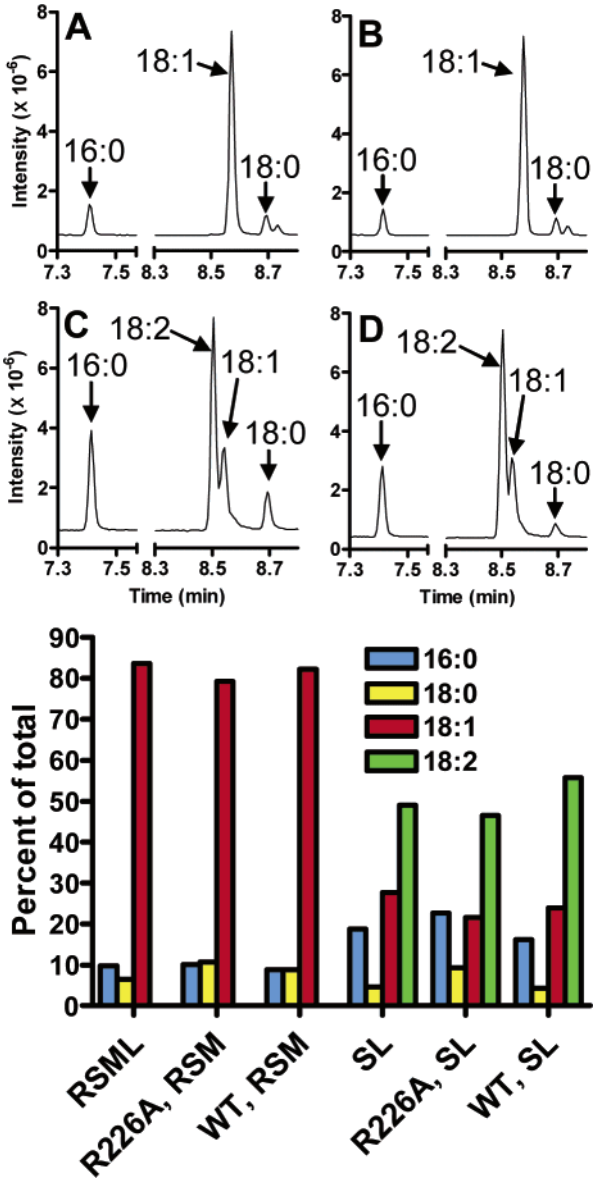

FIGURE 7: Upper panel: Total ion current GC chromatograms showing the separation of methyl esters of fatty acids from extracted lipids. Lipid was extracted and analyzed from the following as described in Materials and Methods: (A) R226A III-His purified from the *R. sphaeroides* membrane; (B) purified *R. sphaeroides* cytoplasmic membranes; (C) R226A III-His purified from soybean lipid vesicles (COVs); (D) purified soybean lipid [L-α-phosphatidylcholine (L-α-lecithin); Sigma]. The methylated fatty acids were identified by mass spectrometry as the following: palmitic acid (16:0) at the retention time of 7.4 min, linoleic acid (18:2) at 8.5 min, oleic acid (18:1) at 8.58 min, and steric acid (18:0) at 8.69 min. A small peak is seen at a retention time of 8.7 min in the samples derived from purified *R. sphaeroides* cytoplasmic membranes and from R226A III-His purified from the bacterial membrane. This compound, which is not present in samples derived from soybean lipid or C*c*O extracted from soybean lipid COVs, was not identified. Lower panel: The fatty acid composition of R226A III-His and WT III-His purified from *R. sphaeroides* membranes or from soybean lipid COVs, compared to the fatty acid composition of bulk *R. sphaeroides* membrane lipids and soybean lipids. The relative amount of each fatty acid is shown as the percent of the total of the four fatty acids identified in the samples by GC/MS. Abbreviations for the samples are as follows: RSML, *R. sphaeroides* membrane lipid; R226A, RSM, R226A III-His purified from *R. sphaeroides* membranes; WT, RSM, WT III-His purified from *R. sphaeroides* membranes; SL, bulk soybean lipid; R226A, SL, R226A III-His purified from COVs; WT, SL, WT III-His purified from COVs.

primary role of subunit III, a highly conserved member of the catalytic core of C*c*O, is to prevent suicide inactivation, thereby extending the lifetime of a membrane protein complex that requires extensive assembly (*42*, *43*). A fundamental finding of this study is that alteration of the conserved binding sites for the two lipids in the cleft of subunit III creates C*c*O forms that inactivate as if subunit III is largely absent, even though the effect is observed in C*c*O preparations in which subunit III is completely retained. Two mutants were examined in depth: W59A-F86A primarily alters the binding site of PE1, while R226A removes the ion pair to PE2. These mutations should disrupt normal lipid binding since inspection of the C*c*O structures shows that the only role of the side chains of Arg-226, Trp-59, and Phe-86 is to bind and position the cleft lipids. Indeed, mutation of Trp-59 and Phe-86 partially disrupts the subunit I−III interface, as described above, presumably by altering lipid binding.

Purification of R226A and W59A-F86A by Ni-affinity chromatography using the histidine tag on subunit III isolates that portion of the mutant population in which subunit III binding has been successful despite disturbance of the lipid binding sites. Thus, purified R226A III-His and W59A-F86A III-His contain stoichiometric amounts of mutant subunits III. As isolated, these mutants showed roughly twice the tendency to suicide inactivate as WT III-His. Incorporation of the R226A III-His and W59A-F86A III-His into vesicles composed of soybean phospholipids (COVs) strongly accentuated their tendency to suicide inactivate, and this behavior was retained after the mutant C*c*Os were either resolubilized from COVs into dodecyl maltoside or reisolated by Ni-affinity chromatography (Table 2). The catalytic life spans of R226A III-His and W59A-F86A III-His after their passage through COVs were 1.8−2.5% of the life span of wild-type C*c*O. In comparison, the life span of C*c*O in which subunit III has been completely removed, measured under these same conditions, is 0.3−0.4% that of the normal enzyme (*14*, *44*). Unlike the lipid binding site mutants, the long catalytic life span of WT III (+) was unaffected by its incorporation into COVs (Table 2). In addition, the catalytic life spans of C*c*O forms with mutations in subunit III outside of the lipid binding sites (S89A I-His, G78S I-His, and A205T I-His) were unaffected by COV incorporation. Thus, the incorporation of C*c*O into COVs, by itself, has no affect on the probability of suicide inactivation.

Apparently, the lipid binding site mutations allow some type of structural alteration to occur when C*c*O is incorporated into COVs, a change that increases the tendency of R226A III-His and W59A-F86A III-His to suicide inactivate by 20−30-fold (Table 2). Possibilities for this structural change include a major loss of subunit III, the removal of PE1 and/or PE2 from the cleft, the exchange of PE1 and/or PE2 for soybean phospholipid, or simply a change in the positions of PE1 and PE2 within their altered binding sites. The loss of subunit III has been ruled out, since both mutants exhibit rapid suicide inactivation in the presence of 100% subunit III, as detailed in Results.

Extensive, if not complete, exchange of bacterial for soybean phospholipids occurs with the passage of C*c*O through COVs (Figure 7). Thus, a large increase in suicide inactivation by the lipid binding site mutants occurs when these proteins are placed in an environment where lipid

exchange and lipid movement take place. Nevertheless, the high number of phospholipids associated with each C*c*O monomer (22 ± 4) precludes a definitive conclusion that the lipids in the cleft of R226A III-His and W59A-F86A III-His are exchanged. Evidence for exchange of the cleft lipids may become possible using more delipidated C*c*O. However, this study deliberately includes no attempts to reduce the number of lipids associated with C*c*O because this could introduce functional changes in addition to those caused by the alteration of the lipid binding sites. Regardless of whether PE1 or PE2 has been lost, exchanged, or merely repositioned as a result of mutating their binding sites and incubating the mutant C*c*Os within a novel lipid bilayer, the results indicate that normal lipid binding sites in the cleft of subunit III are important for the ability of subunit III to prevent suicide inactivation.

Why Does Altering the Lipid Binding Sites Promote Suicide Inactivation? The complete removal of subunit III from C*c*O strongly promotes suicide inactivation (1) by slowing proton delivery to the active site during O_2 reduction and (2) by removing a component of the C*c*O complex that stabilizes the active site during catalytic turnover. It follows that altering the lipid binding sites in the cleft of subunit III, without removing the subunit, must induce suicide inactivation for one, or possibly both, of these reasons. The question of slow proton delivery will be discussed first.

After O_2 binds to reduced heme a_3 in the heme−Cu O_2 reduction site in subunit I, protons enter the heme−Cu site via the D pathway of subunit I from the inner surface of the enzyme (*11*). Slow proton uptake by the D pathway increases the probability of suicide inactivation at the O_2 reduction site, apparently because the slow arrival of protons extends the lifetime of the reactive oxoferryl intermediate ($Fe^{4+}{=}O^{2-}$) and increases the chances that it may hydroxylate nearby residues (*14*). Such side reactions by oxoferryl intermediates have been documented in other proteins (*45*−*47*). The removal of subunit III directly impacts the D pathway, slowing the rate of proton uptake 20-fold at pH 7.4 (*34*).

As detailed in Results, combining the R226A and W59A-F86A mutations with the D132A mutation of subunit I showed that the lipid binding site mutations must increase the probability of suicide inactivation by some mechanism other than (or, possibly, in addition to) any inhibition of the D pathway, since inhibiting the pathway to a greater extent than the D132A mutation itself is extremely unlikely. Comparison of the characteristics of R226A III-His and W59A-F86A III-His to those of D132A III-His alone underscores this conclusion. The alteration of Asp-132, the initial proton donor/acceptor of the D pathway, to alanine slows the most rapid rate of proton uptake by the D pathway by over 3 orders of magnitude, from ∼10000 to ∼5 s^{-1} at pH 7.4 (*12*, *33*). However, the O_2 reduction activity of D132A III (+) at pH 7.4 is ∼30 e^- (also H^+) s^{-1}, somewhat faster than 5 s^{-1} because protons are also delivered to the active site from the outer surface of C*c*O via the proton backflow pathway (*15*, *36*). The catalytic life spans of R226A III-His and W59A-F86A III-His, after COV incorporation and resolubilization, are similar to that of D132A III-His; all three C*c*O forms have life spans of 1−2.5% that of wild-type C*c*O. If slow proton uptake was the sole cause of the increased suicide inactivation exhibited by the lipid binding site mutants, it would be expected that their rates of O_2 reduction would likewise be similar to D132A, i.e., extremely slow. This is not the case. The O_2 reduction activities of R226A III-His and W59A-F86A III-His, post COVs and measured under the same conditions as the measurements of catalytic life span (pH 7.4, 40 μM cytochrome *c*), were 946 ± 20 and 1201 ± 66 e^- s^{-1}, respectively. At a minimum, these turnover rates require an equal rate of proton uptake through the D pathway, rates far greater than that of the D pathway of D132A. Thus, slow proton uptake by the D pathway cannot be the primary source of the short catalytic life spans of the lipid binding site mutants.

Proton backflow from the outer surface of C*c*O partially compensates for reduced proton delivery to the active site when proton uptake from the inner surface, via the D pathway, is inhibited by mutation [e.g., D132A (*33*, *35*)] or by a membrane potential in coupled COVs (*15*, *37*). Inhibition of proton backflow further promotes suicide inactivation when proton uptake via the D pathway is slow (*14*). The removal of subunit III strongly inhibits the proton backflow pathway (*15*). The stopped-flow assays of the rate of controlled and uncontrolled cytochrome *c* oxidation demonstrate that W59A-F86A III-His and R226A III-His have normal rates of proton backflow to the active site (Table 3). Thus, disruption of the cleft lipid binding sites does not affect proton transfer from the outer surface of C*c*O, ruling out a defect in proton backflow as a contributing source for increased suicide inactivation in these mutants.

Normal Lipid Binding Sites in the Cleft of Subunit III Appear To Be Required for Structural Stabilization of the Active Site during Catalytic Turnover. While subunit III is unnecessary for the assembly and stability of subunits I and II in the absence of turnover (*30*), the subunit does supply structural stability to the active site during turnover in terms of decreasing the probability of suicide inactivation. This can be deduced from the following. The catalytic life span of D132A III (+) at pH 7.4 (∼16000 CC; Figure 5) is almost 10-fold greater than that of D132A III (−) [∼2000 CC (*15*, *33*)]. At the same time, proton delivery to the active site of D132A III (+) at pH 7.4 is approximately 10-fold slower than in D132A III (−) [∼30 vs ∼400 s^{-1} (*33*)]. Putting these findings together, it can be seen that subunit III provides considerable protection against suicide inactivation even under conditions (slow proton uptake) that strongly promote suicide inactivation. Given the hypothesis that inactivation results from the hydroxylation of groups at the active site by the oxoferryl intermediate, and the fact that subunit III binds against a large transmembrane surface of subunit I, it seems likely that another way in which subunit III helps to prevent suicide inactivation is by dampening structural oscillations at the active site. In other words, in the absence of subunit III, greater flexibility at the active site increases the probability of a reaction between the oxoferryl intermediate and the surrounding protein.

Since the mutations affecting the lipid binding sites do not induce suicide inactivation by slowing proton delivery to the active site, it seems most likely that they promote suicide inactivation by decreasing the ability of subunit III to provide structural stability to the active site during catalytic turnover. Structural connections between the cleft lipids and a primary target of suicide inactivation, the Cu_B center of the active site (*13*), are seen in the structure of the protein. For example, the terminal carbon of a fatty acid of PE1 is

in van der Waals contact with Leu-243 of helix 5 of subunit I. Ala-242, the neighbor of Leu-243, contacts Pro-285 in helix 6, and Pro-285 is the immediate neighbor of His-284, a Cu_B ligand. Thus, at one point only three residues separate PE1 from a ligand of Cu_B, over a distance of 15.5 Å. This connection from PE1 to Cu_B is structurally conserved from *R. sphaeroides* to bovine C*c*O, except that the cognate of Ala-242 is a serine in bovine C*c*O.

The catalytic cycle of C*c*O requires protein movements at or near the active site, e.g., for alternately directing protons to O_2 reduction or to the proton pump and for the proton pumping mechanism itself (*11*). Reversible dissociation of a histidine ligand of Cu_B may occur with proton pumping (*48*, *49*), and disorder during this event could be the source of the lower pumping efficiency (H^+/e^-) of R226A III-His. It may be that a somewhat flexible buttress for the heme a_3-Cu_B center, in the form of structural lipid, is a structural device that allows movements associated with catalysis to occur, while simultaneously limiting the extent of these movements in order to minimize the probability of suicide inactivation.

ACKNOWLEDGMENT

The authors thank Dr. Laree Hiser and Ms. Elizabeth Graichen for expert assistance in cloning, Dr. Charles Woodley for DNA sequencing, and Drs. Victor Davidson, Larry Prochaska, and Shelagh Ferguson-Miller for valuable comments.

REFERENCES

1. Fyfe, P. K., McAuley, K. E., Roszak, A. W., Isaacs, N. W., Cogdell, R. J., and Jones, M. R. (2001) Probing the interface between membrane proteins and membrane lipids by x-ray crystallography, *Trends Biochem. Sci. 26*, 106−112.
2. Lee, A. G. (2004) How lipids affect the activities of integral membrane proteins, *Biochim. Biophys. Acta 1666*, 62−87.
3. Palsdottir, H., and Hunte, C. (2004) Lipids in membrane protein structures, *Biochim. Biophys. Acta 1666*, 2−18.
4. Lange, C., Nett, J. H., Trumpower, B. L., and Hunte, C. (2001) Specific roles of protein-phospholipid interactions in the yeast cytochrome bc_1 complex structure, *EMBO J. 20*, 6591−6600.
5. Sedlak, E., Panda, M., Dale, M. P., Weintraub, S. T., and Robinson, N. C. (2006) Photolabeling of cardiolipin binding subunits within bovine heart cytochrome *c* oxidase, *Biochemistry 45*, 746−754.
6. Sharpley, M. S., Shannon, R. J., Draghi, F., and Hirst, J. (2006) Interactions between phospholipids and NADH:ubiquinone oxidoreductase (complex I) from bovine mitochondria, *Biochemistry 45*, 241−248.
7. Brzezinski, P. (2004) Redox-driven membrane-bound proton pumps, *Trends Biochem. Sci. 29*, 380−387.
8. Ferguson-Miller, S., and Babcock, G. (1996) Heme/copper terminal oxidases, *Chem. Rev. 96*, 2889−2907.
9. Wikström, M. (2004) Cytochrome *c* oxidase: 25 years of the elusive proton pump, *Biochim. Biophys. Acta 1655*, 241−247.
10. Saraste, M. (1999) Oxidative phosphorylation at the *fin de siecle*, *Science 283*, 1488−1493.
11. Hosler, J. P., Ferguson-Miller, S., and Mills, D. A. (2006) Energy transduction: Proton transfer through the respiratory complexes, *Annu. Rev. Biochem. 75*, 165−187.
12. Ädelroth, P., and Brzezinski, P. (2004) Surface-mediated proton-transfer reactions in membrane-bound proteins, *Biochim. Biophys. Acta 1655*, 102−115.
13. Bratton, M. R., Pressler, M. A., and Hosler, J. P. (1999) Suicide inactivation of cytochrome *c* oxidase: Catalytic turnover in the absence of subunit III alters the active site, *Biochemistry 38*, 16236−16245.
14. Mills, D. A., and Hosler, J. P. (2005) Slow proton transfer through the pathways for pumped protons in cytochrome *c* oxidase induces suicide inactivation of the enzyme, *Biochemistry 44*, 4656−4666.
15. Mills, D. A., Tan, Z., Ferguson-Miller, S., and Hosler, J. (2003) A role for subunit III in proton uptake into the D pathway and a possible proton exit pathway in *Rhodobacter sphaeroides* cytochrome *c* oxidase, *Biochemistry 42*, 7410−7417.
16. Svensson-Ek, M., Abramson, J., Larsson, G., Törnroth, S., Brzezinski, P., and Iwata, S. (2002) The x-ray crystal structures of wild-type and EQ(I-286) mutant cytochrome *c* oxidases from *Rhodobacter sphaeroides*, *J. Mol. Biol. 321*, 329−339.
17. Tsukihara, T., Shimokata, K., Katayama, Y., Shimada, H., Muramoto, K., Aoyama, H., Mochizuki, M., Shinzawa-Itoh, K., Yamashita, E., Yao, M., Ishimura, Y., and Yoshikawa, S. (2003) The low-spin heme of cytochrome *c* oxidase as the driving element of the proton-pumping process, *Proc. Natl. Acad. Sci. U.S.A. 100*, 15304−15309.
18. Sone, N., Yoshida, M., Hirata, H., and Kagawa, Y. (1977) Asolectin purification procedure, *J. Biochem. (Tokyo) 81*, 519−528.
19. Brautigan, D. L., Ferguson-Miller, S., and Margoliash, E. (1978) Mitochondrial cytochrome *c*: Preparation and activity of native and chemically modified cytochromes *c*, *Methods Enzymol. 53*, 128−164.
20. Keen, N. T., Tamaki, S., Kobayashi, D., and Trollinger, D. (1988) Improved broad-host-range plasmids for DNA cloning in gram-negative bacteria, *Gene 70*, 191−197.
21. Bratton, M., Mills, D., Castleden, C. K., Hosler, J., and Meunier, B. (2003) Disease-related mutations in cytochrome *c* oxidase studied in yeast and bacterial models, *Eur. J. Biochem. 270*, 1−9.
22. Brown, B. M., Wang, Z., Brown, K. R., Cricco, J. A., and Hegg, E. L. (2004) Heme O synthase and heme A synthase from *Bacillus subtilis* and *Rhodobacter sphaeroides* interact in *Escherichia coli*, *Biochemistry 43*, 13541−13548.
23. Hiser, L., Di Valentin, M., Hamer, A. G., and Hosler, J. P. (2000) Cox11p is required for stable formation of the Cu_B and magnesium centers of cytochrome *c* oxidase, *J. Biol. Chem. 275*, 619−623.
24. Zhen, Y., Qian, J., Follmann, K., Hayward, T., Nilsson, T., Dahn, M., Hilmi, Y., Hamer, A. G., Hosler, J. P., and Ferguson-Miller, S. (1998) Overexpression and purification of cytochrome *c* oxidase from *Rhodobacter sphaeroides*, *Protein Expression Purif. 13*, 326−336.
25. Hiser, C., Mills, D. A., Schall, M., and Ferguson-Miller, S. (2001) C-terminal truncation and histidine-tagging of cytochrome *c* oxidase subunit II reveals the native processing site, shows involvement of the C-terminus in cytochrome *c* binding, and improves the assay for proton pumping, *Biochemistry 40*, 1606−1615.
26. Cao, J., Hosler, J., Shapleigh, J., Gennis, R., Revzin, A., and Ferguson-Miller, S. (1992) Cytochrome aa_3 of *Rhodobacter sphaeroides* as a model for mitochondrial cytochrome *c* oxidase, *J. Biol. Chem. 267*, 24273−24278.
27. Kovach, M. E., Phillips, R. W., Elzer, P. H., Roop, I. I., R. M., and Peterson, K. M. (1994) pBBR1MCS: A broad-host-range cloning vector, *BioTechniques 16*, 800−802.
28. Flory, J. E., and Donohue, T. J. (1997) Transcriptional control of several aerobically induced cytochrome structural genes in *Rhodobacter sphaeroides*, *Microbiology 143*, 3101−3110.
29. Shapleigh, J. P., and Gennis, R. B. (1992) Cloning, sequencing, and deletion from the chromosome of the gene encoding subunit I of the aa_3-type cytochrome *c* oxidase of *Rhodobacter sphaeroides*, *Mol. Microbiol. 6*, 635−642.
30. Bratton, M. R., Hiser, L., Antholine, W. E., Hoganson, C., and Hosler, J. P. (2000) Identification of the structural subunits required for formation of the metal centers in subunit I of cytochrome *c* oxidase of *Rhodobacter sphaeroides*, *Biochemistry 39*, 12989−12995.
31. Bligh, E. G., and Dyer, W. J. (1959) A rapid method for total lipid extraction and purification, *Can. J. Biochem. Physiol. 37*, 911−917.
32. Mitchell, D. M., and Gennis, R. B. (1995) Rapid purification of wildtype and mutant cytochrome *c* oxidase from *Rhodobacter sphaeroides* by Ni^{2+}-NTA affinity chromatography, *FEBS Lett. 368*, 148−150.
33. Ädelroth, P., and Hosler, J. P. (2006) Surface proton donors for the D-pathway of cytochrome *c* oxidase in the absence of subunit III, *Biochemistry 45*, 8308−8318.
34. Gilderson, G., Salomonsson, L., Aagaard, A., Gray, J., Brzezinski, P., and Hosler, J. (2003) Subunit III of cytochrome *c* oxidase of *Rhodobacter sphaeroides* is required to maintain rapid proton uptake through the D pathway at physiologic pH, *Biochemistry 42*, 7400−7409.

35. Fetter, J. R., Qian, J., Shapleigh, J., Thomas, J. W., Garcia-Horsman, A., Schmidt, E., Hosler, J., Babcock, G. T., Gennis, R. B., and Ferguson-Miller, S. (1995) Possible proton relay pathways in cytochrome *c* oxidase, *Proc. Natl. Acad. Sci. U.S.A. 92*, 1604−1608.
36. Fetter, J., Sharpe, M., Qian, J., Mills, D., Ferguson-Miller, S., and Nicholls, P. (1996) Fatty acids stimulate activity and restore respiratory control in a proton channel mutant of cytochrome *c* oxidase, *FEBS Lett. 393*, 155−160.
37. Mills, D. A., Schmidt, B., Hiser, C., Westley, E., and Ferguson-Miller, S. (2002) Membrane potential-controlled inhibition of cytochrome *c* oxidase by zinc, *J. Biol. Chem. 277*, 14894−14901.
38. Distler, A. M., Allison, J., Hiser, C., Qin, L., Hilmi, Y., and Ferguson-Miller, S. (2004) Mass spectrometric detection of protein, lipid and heme components of cytochrome *c* oxidase from *R. sphaeroides* and the stabilization of non-covalent complexes from the enzyme, *Eur. J. Mass Spectrom. 10*, 295−308.
39. Brooks, C. J., and Middleditch, B. S. (1971) The mass spectrometer as a gaschromatographic detector, *Clin. Chim. Acta 34*, 145−157.
40. Dodds, E. D., McCoy, M. R., Rea, L. D., and Kennish, J. M. (2005) Gas chromatographic quantification of fatty acid methyl esters: Flame ionization detection vs. Electron impact mass spectrometry, *Lipids 40*, 419−428.
41. Kurata, S., Yamaguchi, K., and Nagai, M. (2005) Rapid discrimination of fatty acid composition in fats and oils by electrospray ionization mass spectrometry, *Anal. Sci. 21*, 1457−1465.
42. Carr, H. S., and Winge, D. R. (2003) Assembly of cytochrome *c* oxidase within the mitochondrion, *Acc. Chem. Res. 36*, 309−316.
43. Smith, D., Gray, J., Mitchell, L., Antholine, W. E., and Hosler, J. P. (2005) Assembly of cytochrome *c* oxidase in the absence of assembly protein Surf1p leads to loss of the active site heme, *J. Biol. Chem. 280*, 17652−17656.
44. Hosler, J. P. (2004) The influence of subunit III of cytochrome *c* oxidase on the D pathway, the proton exit pathway and mechanism-based inactivation in subunit I, *Biochim. Biophys. Acta 1655*, 332−339.
45. Kinzie, S. D., Thevis, M., Ngo, K., Whitelegge, J., Loo, J. A., and Abu-Omar, M. M. (2003) Posttranslational hydroxylation of human phenylalanine hydroxylase is a novel example of enzyme self-repair within the second coordination sphere of catalytic iron, *J. Am. Chem. Soc. 125*, 4710−4711.
46. Farquhar, E. R., Koehntop, K. D., Emerson, J. P., and Que, L., Jr. (2005) Post-translational self-hydroxylation: A probe for oxygen activation mechanisms in non-heme iron enzymes, *Biochem. Biophys. Res. Commun. 338*, 230−239.
47. Koehntop, K. D., Marimanikkuppam, S., Ryle, M. J., Hausinger, R. P., and Que, L., Jr. (2006) Self-hydroxylation of taurine/alpha-ketoglutarate dioxygenase: Evidence for more than one oxygen activation mechanism, *J. Biol. Inorg. Chem. 11*, 63−72.
48. Sharpe, M., Qin, L., and Ferguson-Miller, S. (2005) Proton entry, exit and pathways in cytochrome oxidase: Insight from "conserved" water, in *Biophysical and Structural Aspects of Bioenergetics* (Wikström, M., Ed.) pp 26−54, Royal Society of Chemistry, Cambridge, U.K.
49. Wikström, M. (2000) Mechanism of proton translocation by cytochrome *c* oxidase: A new four-stroke histidine cycle, *Biochim. Biophys. Acta 1458*, 188−198.

BI061390Q